editors

Fritz Herlach

Noboru Miura

High Magnetic Fields

Science and Technology

Theory and Experiments II

Vol. 3

High Magnetic Fields

Science and Technology

Theory and Experiments II

Vol. 3

editors

Fritz Herlach

Laboratorium voor Vaste-Stoffysika en Magnetisme,
Katholieke Universiteit Leuven, Belgium

Noboru Miura

Institute for Solid State Physics, University of Tokyo, Japan

World Scientific

NEW JERSEY • LONDON • SINGAPORE • BEIJING • SHANGHAI • HONG KONG • TAIPEI • CHENNAI

Published by

World Scientific Publishing Co. Pte. Ltd.

5 Toh Tuck Link, Singapore 596224

USA office: 27 Warren Street, Suite 401-402, Hackensack, NJ 07601

UK office: 57 Shelton Street, Covent Garden, London WC2H 9HE

British Library Cataloguing-in-Publication Data
A catalogue record for this book is available from the British Library.

HIGH MAGNETIC FIELDS: SCIENCE AND TECHNOLOGY (Vol. 3)

ISBN 981-02-4964-0 (Vol. 1)
ISBN 981-02-4965-9 (Vol. 2)
ISBN 981-02-4966-7 (Vol. 3)
ISBN 981-02-4698-6 (Set)

Printed in Singapore by World Scientific Printers (S) Pte Ltd

High Magnetic Fields

Science and Technology

PREFACE

The magnetic field is a basic research tool in physics, with most applications in solid-state physics. Apart from the exciting aspect of advancing into uncharted territory where new effects are waiting to be discovered, higher fields provide both increased resolution and sensitivity. The Physics Nobel Prize for the discovery of the quantum fluid in high magnetic fields by Laughlin, Störmer and Tsui is one of the recent highlights. "Very high fields" are loosely defined as requiring special and some very large magnet laboratory facilities. Since the last comprehensive book on experiments with high magnetic fields was published in 1985 (Strong and Ultrastrong Magnetic Fields and Their Applications, ed. F. Herlach, Springer Topics in Applied Physics), very substantial progress has been made in magnet technology and experimental methods, and a wealth of experimental results has been accumulated. This is reflected in the size of the present survey that consists of three volumes, one on magnet technology, facilities and experimental techniques, and two on experiments and theory of physics and related topics in high magnetic fields.

In magnet technology, 33 T water-cooled magnets and a 45 T hybrid magnet have become operational at the U.S. National High Magnetic Field Laboratory at Tallahassee, and the new Nijmegen magnet laboratory is now in operation. Several new laboratories with pulsed magnets have been established, and existing laboratories have been upgraded and modernised. The level of non-destructive "user" fields has been raised from 50 to 70 T, and 80 T is becoming available as the result of a European co-operative project. The HLD at Dresden is nearing completion, adding a new dimension to pulsed field laboratories. Several single-turn coil installations have been built at Tokyo and Berlin that provide fields up to 300 T, and in electromagnetic compression it has recently become possible to generate 600 T reproducibly (at the University of Tokyo). Fields up to 1000 T from explosive-driven flux compression have become available at Sarov (Russia) and Los Alamos (partner of NHMFL). For pulsed magnetic fields in particular, new experimental techniques have been developed with unprecedented resolution and sensitivity, enabling experiments that two decades ago would have been considered a remote dream.

The present volume contains a chapter on organic conductors that is complementary to that in Vol. 2. Another complementary chapter is that on high temperature superconductors, where pulsed magnets provide an opportunity to finally resolve the puzzle of the mechanism that leads to high T_c superconductivity. In addition to those in Vol. 2, there is another chapter on magnetic interactions, and one on permanent magnetism. Magnetism is a very wide field with a long tradition in high-field research and with large-scale practical applications. Two chapters cover different aspects of semiconductor physics, one on two-dimensional systems and one on cyclotron resonance. These confirm that semiconductor physics is still in the mainstream of modern solid state physics in high magnetic fields. Nuclear magnetic resonance has greatly benefited from the development of high field magnets, obtaining high levels of resolution and sensitivity. One chapter in this volume is dedicated to NMR in solids using the highest fields presently available for this purpose. In the comprehensive chapter on biological systems, NMR is only one of many methods used to study systems related to living organisms. Then, there is a chapter on plasma physics

where once there was great hope to achieve fusion by using very strong magnetic fields. Although emphasis has now shifted to very large toroidal steady-state devices, pulsed fusion with very strong magnetic fields may turn out to be a viable alternative to obtain fusion energy in smaller machines. The final chapter is another absolute highlight; it deals with the extremely high fields that have been discovered in the universe. This also provides an excellent insight into related theoretical considerations.

Each chapter provides a tutorial introduction followed by an in-depth discussion of recent experiments and theory with a view to future developments. We hope that these volumes will be useful as a stimulus as well as a reference tool for researchers and engineers working with high magnetic fields, and for students who want to become familiar with this field of research.

Volume 1 contains a survey of magnet laboratories. Since it was published two years ago, the addresses of several laboratories have changed, and web-sites have been added. An update on the addresses is given in the appendix.

CONTENTS

QUASI-ONE-DIMENSIONAL ORGANIC CONDUCTORS IN HIGH MAGNETIC FIELDS

J.S. BROOKS
NHMFL/Physics, Florida State University, Tallahassee FL 32310 USA
E-mail: brooks@magnet.fsu.edu

O.H. CHUNG
Department of Physics, Sunchon University, Sunchon, Chunnam 540-742 South Korea
E-mail: ohchung@sunchon.ac.kr

We review the mechanisms and physical properties of quasi-one-dimensional (Q1D) conductors in high magnetic fields. Low dimensional materials are susceptible to instabilities which lead to broken symmetry ground states, including charge density wave, spin density wave, and superconductivity. Since the characteristic temperatures of phase transitions are often relatively low, the corresponding magnetic fields where profound changes in their ground states can occur are within the range of accessible dc and pulsed magnetic fields. We focus on more recent work and on Q1D systems that are not yet well known in the popular literature.

1 Introduction

Electronically anisotropic, quasi-one-dimensional (Q1D) organic materials in the charge transfer class, together with their many ground states, have been the subject of active study for more than 20 years, especially since the discovery of superconductivity in $(TMTSF)_2PF_6$ by Jerome and co-workers [1]. Quite often, the discovery of superconductivity somehow "anoints" a new material as interesting and worthy of further study. The superconducting ground state tells us that many body effects are important, and that other phenomena or ground states may be in close proximity. These are generally accessible with a little push with pressure, chemistry, or magnetic field. This grows even more interesting in highly anisotropic materials, where the the electronic states may become physically confined in one or more directions. Indeed, it was pressure that induced superconductivity in the otherwise insulating spin density wave (SDW) ground state of $(TMTSF)_2PF_6$, which at ambient pressure results from a Q1D instability. The importance of high magnetic fields came closely on the heels of this discovery since the nature of the critical field is necessary to describe the essential details of superconductivity: coherence length, penetration depth, H_{c1}, H_{c2} for the vortex lattice, and $H_{\rm Pauli}$ for the field carefully aligned in-plane for these low dimensional materials. But, superconductivity was only the beginning of the story, since high magnetic fields revealed a new world of low dimensional physics, primarily due to the close proximity of Zeeman, orbital (either closed or transverse), electronic (imperfect nesting - see below), and transition temperature energy scales.[a] There is a vast literature on low-dimensional organic metals, which is very thoroughly treated in the undisputed classic book by Ishiguro, Yamaji, and Saito [2]. Since it would be futile to try to repeat the material in this as in other

[a] For a typical Q1D organic metal with a density wave transition of order 12 K ($T_{\rm DW}$), at 30 T (easily obtained at any modern high field laboratory) these energies are $\mu_B H = 1.74$ meV, $\hbar\omega_c = 3.5$ meV, $\hbar\omega_b = 4.5$ meV, $t'_b = 0.5$ meV, $T_{\rm DW} = 1.0$ meV.

Table 1: Transfer integrals and possible low temperature ground states for representative Q1D compounds (parameters from Ref. [2]). Here a, b and c refer to the principal crystallographic axes.

	$(TMTSF)_2PF_6$	$(TMTTF)_2X$	$(Per)_2M(mnt)_2$	$(DMET\text{-}TSeF)_2AuCl_2$
t_x (meV)	300 (a)	250(a)	150 (b)	420 (a)
t_y (meV)	25 (b)	10(b)	2(a)	64(b)
t_z (meV)	1 (c)	1 (c)	0 (c)	-
ground states	SDW, SC, FISDW	CL, SP, SDW	CDW	SC, FISDW

major reviews [3–6], we will try to focus only on those issues and phenomena that are most relevant to Q1D in high magnetic fields. We will focus on several distinctly different Q1D systems that have been the subject of high magnetic fields, and which also test different aspects of our understanding of the physics of Q1D materials. Useful formulae relevant to the understanding and analysis of the properties of Q1D materials in magnetic fields will likewise be presented.

2 Electronic Structure of Quasi-One-Dimensional Materials

In Fig. 1, we have tried to capture the main aspects of the Q1D scenario. Q1D conductors are really three-dimensional materials, it is just that the bandwidth between molecules within the conducting chains (t_a) is much larger than that between the chains (t_b), which, in turn, is larger than that between the (really two-dimensional) layers consisting of parallel chains (t_c). In Table 1, the transfer integrals for a representative group of materials to be discussed in this report and their possible ground states are shown.[b]

From the transfer integrals, the tight binding model leads to a simplified dispersion relation

$$\epsilon(\vec{k}) = -2t_a\cos(ak_x) - 2t_b\cos(bk_y) - 2t_c\cos(ck_z) \tag{1}$$

where a, b, and c are lattice parameters along the x, y, and z-axis, respectively.[c] In the case of Q1D anisotropy where we neglect the inter-layer bandwidth t_c, this reduces to (after Hasegawa and Fukuyama [7])

$$\epsilon(\vec{k}) = v_x(\mid k_x \mid -k_F) - 2t_b\cos(bk_y) + 2t_b'\cos(2bk_y) \tag{2}$$

where

$$v_x = \frac{2at_a}{\hbar\sin(ak_F)} \quad \text{and} \quad t_b' = \frac{t_b^2\cos(ak_F)}{4t_a\sin^2(ak_F)} \ . \tag{3}$$

[b] It is worth noting that for bulk crystals, the molecular and lattice vibrational modes always have three-dimensional degrees of freedom.

[c] In many Q1D materials, the a, b, and c axes refer to the intrachain (x), interchain (y), and interplane (z) directions, and we will generally follow this convention. Likewise, the unit cell axes may not be normal to the crystallographic planes (b', c^*, etc.) but we will use the a, b, and c notation for simplicity with this understanding.

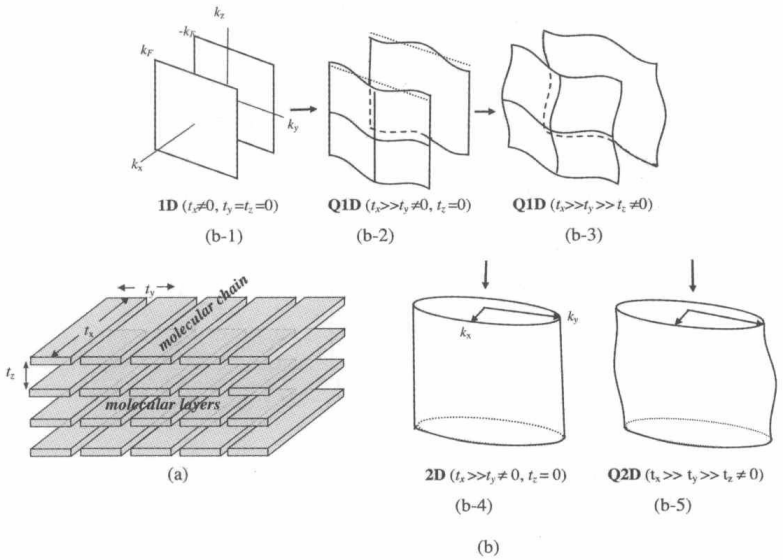

Figure 1: (a) Schematic representation of a typical quasi-one-dimensional crystal structure. (b) Evolution of the Fermi surface for various combinations of transfer integrals (t_x,t_y, and t_z) for 1D and 2D systems.

The Fermi surface (FS) is then described by

$$k_x = \pm(k_F + (2t_b \cos(bk_y) - 2t_b^{'} \cos(2bk_y))/\hbar v_x) \ . \tag{4}$$

The term $t_b^{'}$ above is called the imperfect nesting parameter. If we neglect it in Eq. (4), the resulting FS will be two purely sinusoidal sheets at $\pm k_F$ as shown in Fig. 2. By transposing the $-k_F$ sheet by a factor of $2k_F$ to $+k_F$, and shifting it up by π/b, the two FS sheets will exactly overlap. This is called perfect nesting and the vector of transposition is the perfect nesting vector $\vec{Q}_0 = (2k_F, \pi/b)$. As discussed below, this will lead to a fully gapped system at the Fermi level. However, when $t_b^{'}$ increases, then higher order terms appear in the dispersion and it is not possible for $\vec{Q}_0$ to gap all the FS. Eventually, for $t_b^{'} = k_B T_{\rm SDW}$, the nesting will be too small to stabilize a density wave state. This is depicted in Fig. 2 where the dependence of the reduced ordering temperature is shown vs. the variation of the imperfect nesting parameter. The inset curves are the $+k_F$ sections of the $\vec{Q} = (2k_F, \pi/b)$ nested FS for $t_a = 250$ meV, and t_b for the range 10, 15, 20, and 24 meV, where $t_{b'}$ is computed from Eq. (3) above for a $T_{\rm SDW}$ of 12 K.[d] Here $t_{b0}^{'}$ corresponds to the critical imperfect nesting factor for stabilizing a spin density wave(SDW) phase at 0 K and evaluated as $T_{\rm SDW}^0/1.13$ where $T_{\rm SDW}^0$ is the temperature for perfect nesting (e.g. $t_{b'} = 0$). Electron and hole pockets arise as a result of imperfect nesting. As Fig. 2 shows, the changes in Fermi surface topology due to the degree of imperfect nesting which can destroy the SDW phase are very small, compared with the b-axis bandwidth.

[d]The values for an actual material will depend on the band filling, nesting vector, etc.

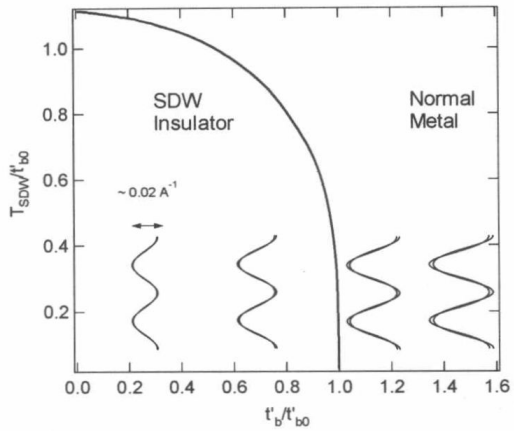

Figure 2: Stability of a SDW ground state versus the imperfect nesting parameter t'_b/t'_{b0}. Nested FS sheets (for $+k_F$ only) are shown for increasing t_b for $t_a = 250$ meV and $m* = 1.0\,m_0$ following Eqs. (1)–(4) (see text for details).

3 The Effect of High Magnetic Fields on Q1D Systems

The primary mechanism by which the magnetic field interacts with a Q1D is through Zeeman and orbital coupling. The Zeeman term, which acts on the π electron system, will always be present. The relationships between the nesting vectors and the spin-split bands are shown in Fig. 3 for both the spin density wave (SDW) and charge density wave (CDW) pairing states for a simple 1D band configuration. In CDW systems, the field acting through the Pauli susceptibility, will destroy (in the absence of orbital coupling) the CDW ground state. However, for a SDW system [8], the optimum nesting vector does not change as the bands split. For a superconducting ground state, if the field is carefully aligned in the conducting plane of a material with negligible interplane coupling $t_z \sim 0$, the vortex lattice is suppressed, and the superconducting ground state will be governed only by Pauli or other non-vortex mechanisms.

In the normal state, the orbital coupling is through the Lorentz force $\hbar\partial\vec{k}/\partial t = e\vec{v}_k \times \vec{B}$, where the electron dynamics in magnetic field are obtained through the Landau–Peierls substitution $\vec{k} \rightarrow \vec{k} - e\vec{A}/\hbar$. In a Q1D picture, $\vec{A} = (0, H_x, 0)$ is generally used in the Landau gauge. Orbital effects depend on the degree to which the material deviates from a strictly one-dimensional chain, as shown for different relative transfer integral values in Fig. 1(b). For $t_x \neq 0, t_y = t_z = 0$ in our notation, there are only two parallel Fermi surface sheets (Fig. 1(b-1)), the electron motion is strictly confined to each single chain, and the magnetic field has no orbital effect. For $t_x \gg t_y \neq 0, t_z = 0$, the real space electron orbit will move along the chains with oscillatory spatial motion in the y direction (Fig. 1(b-2)) due to the Lorentz force. Here, an electron with Fermi velocity v_F along the x-direction in the presence of a magnetic field will cross the Brillouin zone in the y-direction with frequency $\omega_b = ev_F Hb/\hbar$ as depicted in Fig. 4(a). The amplitude of the y motion will decrease with increasing magnetic field, thereby, driving the oscillatory motion more one-

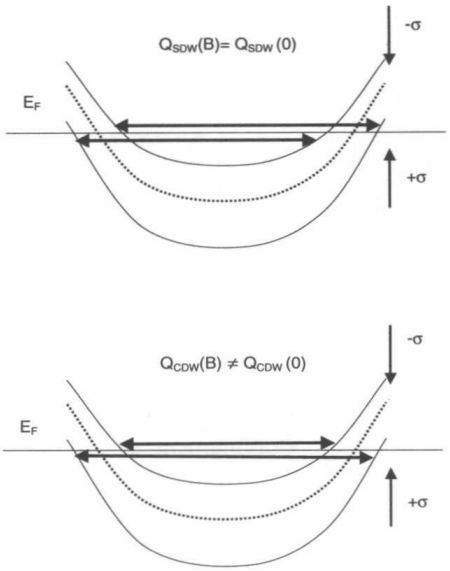

Figure 3: Scenarios for nesting at the Fermi surface for finite magnetic field. Dashed lines represent the zero magnetic field bands, where the nesting vector in both cases is just $2k_F$. (a) For SDW nesting with $\sigma_\uparrow$ $\sigma_\downarrow$ electron-hole pairing, the nesting vector does not change from $Q_{\rm SDW}(0) = 2k_F$ with increasing field. (b) For CDW nesting with $\sigma_\uparrow$ $\sigma_\uparrow$ and $\sigma_\downarrow$ $\sigma_\downarrow$ electron-hole paring, the nesting vectors increase (decrease) from $Q_{\rm CDW}(0) = 2k_F$ continuously with increasing field.

dimensional. Chaikin has given an intuitive description which describes this process [3]. This approach yields the real-space amplitude $A_y = 4bt_b/\hbar\omega_b$ and wavelength $\lambda_x = h/eHb$ of the real-space motion of a carrier in the direction of the conducting chains (see Fig. 4).

We note that, not until a field of order 1000 T is reached, will the carrier be confined within a single chain. However, for a metallic Q1D system, a field of order 10 T (where A_y and λ_x are still much larger than the lattice constants) is sufficient to induce a SDW state. A detailed description of how CDW and SDW ground states emerge in a Q1D system, and, moreover, how a magnetic field can induce a SDW ground state [9] is beyond the scope of this report. However, we can summarize the essential features as follows: Both the CDW and SDW ground states are the result of a rearrangement of the charge, spin, and lattice parameters to lower the free energy of the Q1D system. For low on-site repulsion $U \ll t_a$, a CDW is favored, but when the on-site repulsion is stronger ($U \approx t_a$), a SDW is favored. As shown in Fig. 3, a characteristic nesting vector of order $2k_F$ connects opposite Fermi surface sheets, and for any perturbation at this wave number the instability will arise. Theoretically, when the computed generalized susceptibility $\chi(\vec{Q})$ diverges for a particular value of $\vec{Q}$, this is an indication of an instability for that nesting vector. The divergence decreases as the dimensionality of the system increases. In $(TMTSF)_2ClO_4$ at low temperatures, the imperfect nesting is too large for a SDW state to develop, and the optimum nesting vector $\vec{Q} = (2k_F, \pi/b)$ cannot produce a gap. However, in finite field a new component of the k_x wave vector, $\kappa = eHb/\hbar$, (i.e., $2\pi/\lambda$ as given above) arises. Indeed,

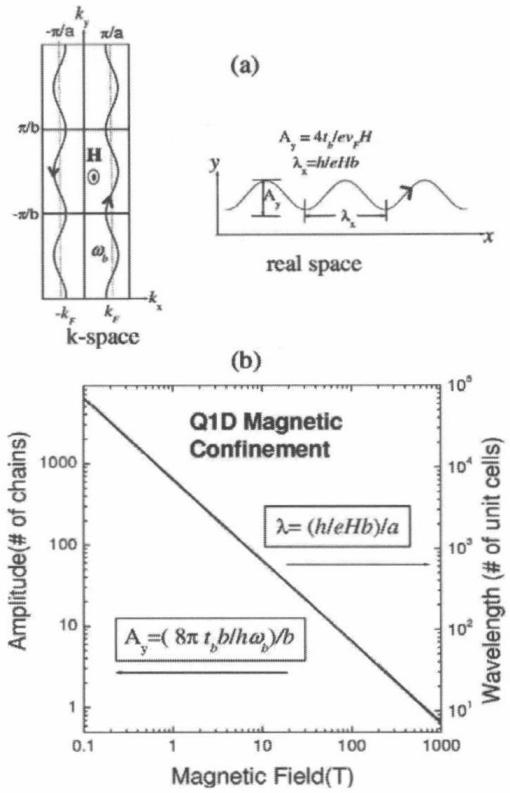

Figure 4: (a) Semiclassical motion of Q1D electrons in k-space and real space in the presence of a magnetic field (after Ref. [3]). (b) Variation of the electron orbital amplitude (in the inter-chain direction) and wavelength (along the chains) with magnetic field $H \parallel z$.

when $\vec{Q} = (2k_F + \kappa n, \pi/b)$, where n is an integer, $\chi(\vec{Q})$ can exhibit singularities, and the SDW can be stabilized, leading to a field induced SDW (FISDW) state. In the simple language of the Q1D Fermi surface topology, if the nesting is bad for $\vec{Q} = (2k_F, \pi/b)$, then if one shifts the nested sheet a bit more in the k_x direction by κn, part of the FS can be well nested. The second, and equally important part of this process is that the un-nested sections of the FS will produce closed pockets with quantized area $2\pi eH/\hbar$. When the spin and orbital energies are considered, this configuration, which leads to a FISDW state, is the lowest energy ground state[9]. Since κ increases linearly with field, this also leads to quantum cascade features in the FISDW. The Fermi level stays in between the Landau levels of the pockets (the energy is lowered by having all Landau levels filled below E_F), and this gives rise to a quantum Hall effect [10–13].

For $t_x \gg t_y \gg t_z \neq 0$ (Fig. 1(b-3)), the oscillatory motion can occur as well along the z-axis. In this case, geometric resonance effects can arise for magnetic field tilted along certain crystallographic directions, leading to magic angle effects. For Q1D metals,

a commensurate effect of the electron motion between b- and c-directions is observable at magic angles in magnetoresistance in tilted fields in the bc-plane, as Lebed pointed out first [14]. The condition for Lebed oscillations in triclinic structure, an evidence of the Q1D system, is given by the condition

$$\tan(\theta) = \frac{p}{q} \cdot \frac{b \sin \gamma}{c \sin \beta \sin \alpha} - \cot \alpha^* \tag{5}$$

where p and q are integers and b, c, α, β, and γ are lattice parameters of the crystal. As can be seen from Eq. (5), the physical information from the AMRO effect in Q1D system is purely related to the geometry of crystal structure and not to topology of 1D bands (Fig. 6). If the y dispersion is sufficiently large to close the Fermi surface, or, if crystallographic ordering effects or nesting fold the Q1D Fermi surface, then cyclotron orbits due to electron and hole pockets can arise, and the system becomes quasi-two-dimensional (Q2D) as depicted in Fig. 1 (b-4) and (b-5). As will be more fully discussed in Sec. 3.4 below, quantum oscillations associated with the de Haas-van Alphen effect will occur, and in tilted magnetic fields Q2D resonances associated with the warped Q2D Fermi surface (Yamaji–Kajita–Kartsovnik effects [15,16]) can be observed.

All of the above are called as the semi-classical Boltzmann transport effects. More exotic possibilities for electronic transport will be discussed in a subsequent section. But let's first discuss the basic phenomena in magneto-transport in real Q1D systems, where unless otherwise specified, we assume the field is perpendicular to the most conducting molecular plane.

3.1 A Simple Q1D Metal in High Magnetic Fields

We begin our exposition of Q1D materials in high fields with the (DMET-TSeF)$_2$AuCl$_2$ class of materials [17]. These are characterized by their asymmetric donor character and their linear anion structure, $AuCl_2$, AuI_2 (superconducting), $AuBr_2$, or I_3 (no FISDW). Since no anion ordering occurs in these materials, the Fermi surface at low temperatures retains the simple open topology of a Q1D FS as depicted in Fig. 1(b). Hence, in principle, these materials should capture the essential aspects of a Q1D metal in high magnetic fields.

An example of the magnetic field dependent properties [18] of (DMET-TSeF)$_2$AuCl$_2$ is shown in Fig. 5. Although in a strictly 1D system there is no magnetoresistance for finite interchain bandwidth, a slightly superlinear MR is generally observed. At higher magnetic fields a series of features appear, which are field-induced spin density wave (FISDW) transitions. These are the result of the orbital confinement mechanism [9,19] which drives the system towards 1D instabilities. Here, a quantized FISDW gap opens over part of the Fermi surface, and the resistance rises. Superimposed on the FISDW structure is the appearance of so-called rapid oscillations. The frequencies of these oscillations are generally in the range of 200 T. Although not universally accepted, we believe that the rapid oscillations are the result of Q2D pockets that result from a reconstructed Q1D Fermi surface, either by anion ordering (see Fig. 7 below), or by field induced nesting (see Fig. 3). To our knowledge, rapid oscillations have never been observed in an open orbit, strict Q1D system without nesting or reconstruction.

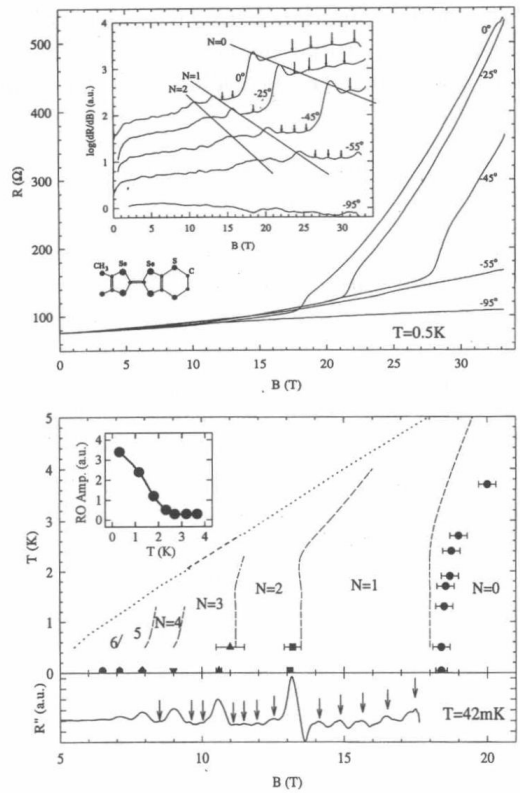

Figure 5: Magnetic field dependence of the asymmetric system (DMET-TSeF)AuI_2 (after Ref. [18]). Upper panel: Angular dependent magnetoresistance (MR) study of the FISDW behavior. Inset: log-derivative of the MR showing the rapid oscillation (RO) and FISDW details. Lower panel: SDW temperature-magnetic field phase diagram for $\theta = 0$. Dashed lines are for the corresponding SDW phases in $(TMTSF)_2PF_6$. Lower inset shows the second derivative of the MR and the RO behavior. Upper inset indicates the temperature dependence of the RO amplitudes, which increase monotonically with lower temperatures.

As the magnetic field is tilted into the conducting planes of the material, the positions of the FISDW and RO positions follow a $1/\cos(\theta)$ dependence, which is characteristic of a Q2D orbital system. Deviations from this behavior have been observed in the FISDW state, and have been attributed to a sliding of the FISDW state in tilted magnetic fields. The temperature dependence of the rapid oscillations in the $(DMET\text{-}TSeF)_2AuCl_2$ system monotonically increases with lower temperatures, which is characteristic of a Q2D quantum oscillation amplitude. As noted below, the temperature dependence becomes more complicated in other Q1D materials with SDW ground states. The angular dependent magnetoresistance (AMRO) for several of the $(DMET\text{-}TSeF)_2X$ systems [20] is shown in Fig. 6. This phenomenon, known as the "Lebed" effect, follows the behavior described above for Eq. (5). Here features in the magnetoresistance for a constant magnetic field vs. angular rotation in the plane perpendicular to the conducting chains reveal structure for field directions that

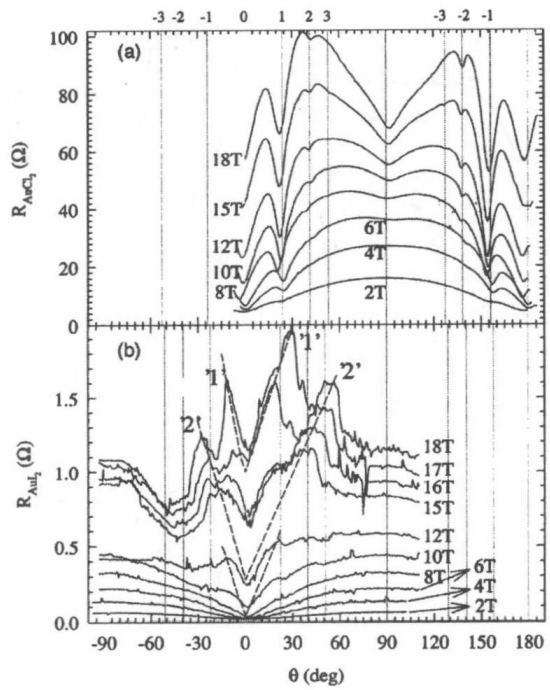

Figure 6: Angular dependent magnetoresistance effects in $(DMET\text{-}TSeF)_2X$ for X = $AuCl_2$ (upper panel) and X = AuI_2 (lower panel) for different magnetic fields. θ is the angle of the magnetic field from the b-axis. Vertical lines represent the Lebed angles calculated from the lattice parameters and labelled as p/q according to Eq. (5). Numbers in quotes indicate the FISDW index corresponding to each maxima. Broken lines are guides for the eye for the shift of these maxima (after Ref. [20]).

involve integer ratios of the lattice constants in the y and z directions. This type of behavior is specific to Q1D systems. As discussed below, for a Q2D system, the relevant parameter is the product of the interplane lattice constant z and the Fermi momentum k_F.

In summary of this section, the DMET class of materials give a simple description of Q1D physics in high fields where complications due to anion ordering are not present.

3.2 A Q1D Metal with Fermi Surface Reconstruction

Q1D systems, where anion ordering can occur, will cause doubling of the unit cell in one or more directions, resulting in a reconstruction of the Fermi surface. Q1D $(TMTSF)_2X$ materials with low symmetric tetrahedral anions such as ClO_4, ReO_4, and FSO_3 will generally undergo anion ordering below a characteristic temperature T_{AO}, which for $(TMTSF)_2ClO_4$ is 24 K. Although randomly oriented at room temperature, the tetrahedral anions order in an up, down, up, down arrangement, and this doubles the unit cell along the b-axis direction, resulting in a new reciprocal lattice $(k_a, k_b/2, k_c)$ or more simply $(0, \frac{1}{2}, 0)$ as depicted in the bottom of Fig. 7 (as will be discussed in Sec. 3.4, the reconstruction can be modified

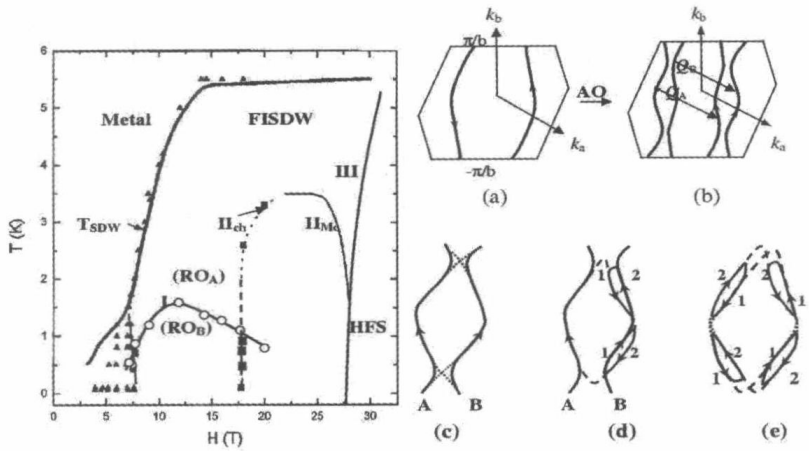

Figure 7: Left: Detailed picture of the FISDW phases for $(TMTSF)_2ClO_4$ **I**: $T^*(H)$ by Chung *et al.*[26] $\mathbf{II}_{Mc}$: McKernen's 3.5 K phase boundary in the FISDW state[21]. The main metal-to-FISDW phase boundary is shown by TSDW , where at low temperatures a cascade of transitions are seen below 8 K. At higher fields below TSDW new phase boundaries appear due to the complexity of the nesting phenomena, as determined from the RO behavior and other anomalies in the magnetoresistance: $\mathbf{II}_{ch}$: low field side extension of II_{Mc} **III**: High field state boundary. Bottom: (a) FS of a normal Q1D metal. (b) FS of metallic state with AO along the b'-axis. Here Q_A and Q_B are two possible SDW nesting vectors. (c) The Stark interference oscillation between two parallel electron motions. (d) Coexistence of SDW_A nesting with Q_A and metallic FS. (e) Small electron and hole pockets are formed after both SDW nestings occur.

by pressure). This results in "folding" the Fermi surface sheets inwards in the reduced zone scheme Fig. 7(b). Since there are now four Q1D Fermi surface sheets, the magnetotransport behavior becomes more complicated.

It is important to note that for anion ordering, the cooling rate is of enormous importance. For $(TMTSF)_2ClO_4$, a cooling rate of a few mK per minute through the 24 K transition is sufficient to produce a well ordered ground state, which is metallic and superconducting. However, as the cooling rate is increased, there will be systematically more disorder in the material, and this can lead to additional, complicated behavior in the magnetotransport phenomena[22]. In an extreme case where $(TMTSF)_2ClO_4$ is thermally quenched (Q-ClO_4), there is no anion ordering, the simple Q1D FS remains, and a SDW state occurs below 5 K (see Sec. 3.3). A rapid oscillation (RO) frequency is observed in the SDW state with a frequency of 190 T[23]. In $(TMTSF)_2PF_6$, where there is also no anion ordering and a SDW below 12 K, Ulmet and co-workers[24] first discovered RO with a frequency of about 220 T. In these latter two cases, the RO amplitudes are non-monotonic in temperature, with a maximum in the range 1 to 3 K below T_{SDW}. The RO behavior in the case of $(TMTSF)_2ClO_4$ is very complicated, as treated in study of $(TMTSF)_2ClO_4$ by Uji *et al.*[25] and Chung *et al.*[26], as depicted in Fig. 8. Unlike the situation for $(DMET\text{-}TSeF)_2AuCl_2$ above with no FS reconstruction, quantum oscillations with frequency $F \simeq 260$ T are observed in the metallic phase of $(TMTSF)_2ClO_4$ outside the FISDW transition. Based on the reconstructed Fermi surface topology due to anion ordering as shown in Fig. 7(b), these oscillations are thought